BLUFF BODY FLOWS IN THE PRESENCE OF A FREE SURFACE

Thesis by
Siddhartha Valluri

In Partial Fulfillment
of the Requirements for the Degree of
Doctor of Philosophy

California Institute of Technology
Pasadena, California

1996

(Submitted October 9, 1995)

ACKNOWLEDGMENTS

I am deeply indebted to my advisors Prof. Anatol Roshko and Mory Gharib for giving me an opportunity to come to Caltech and work with them. It has been a unique privilege to have them as mentors and friends. Their unstinting support and enthusiasm for all my endeavors has been an immense source of encouragement.

I would like to express my appreciation to my colleagues Derek Lisoski and Flavio Noca for their constant support, advice, help and friendship. The time they spent lessening my ignorance undoubtedly added to their tenure at GALCIT. Thanks are also due to Dana Dabiri and Steve Haase for all their help.

I would also like to thank Hans Hornung, Tony Leonard and Ted Wu for graciously agreeing to be on my thesis committee.

This work was supported by the Office of Naval Research URI program "Interaction of Vorticity with a Free Surface" Grant No. N00014-91-J-1610.

Dedicated to my teachers at St.Joseph's Boys' High School who taught me to think

ABSTRACT

An experimental study is performed in a water tunnel (Re = 40,000 to Re = 60,000) to study the interaction between the wake of a circular disk and the free surface. The deformation of the free surface is correlated with the behavior of the wake by utilizing surface pictures, wake flow visualization, drag measurement and Digital Particle Image Velocimetry techniques. It is observed that the wake can exist in two modes with different stabilities. The flow can switch between these two modes and the switching process exhibits hysteresis. The topological differences between these modes and their relation to the observed surface patterns are discussed. The changes in the wake are reflected by an increase in Cd which reaches a maximum value when the upper edge of the disk is 0.125 diameters from the surface. Comparison is also made with a disk approaching a solid boundary.

TABLE OF CONTENTS

TABLE OF FIGURES

NOMENCLATURE

$\uparrow$	-	Denoting upward motion of the disk
$\downarrow$	-	Denoting downward motion of the disk
ρ	-	Fluid density
υ	-	Kinematic viscosity
Cd	-	Drag coefficient ($\frac{D}{\frac{1}{2}\rho S U_\infty^2}$)
Cd_{norm}	-	Cd normalized to the fully submerged value (~ 1.3)
D	-	Drag
d	-	Diameter of the disk
h	-	Distance from upper edge of disk to the undisturbed free surface level
Fr	-	Froude Number ($U_\infty / \sqrt{gh}$)
M1	-	Mode-1
M2	-	Mode-2
Re	-	Reynolds Number ($\frac{d U_\infty}{\upsilon}$)
S	-	Surface area of the disk ($\frac{\pi d^2}{4}$)
s	-	Distance of forward stagnation point from the center of the disk
U_∞	-	Free stream velocity

1. Introduction

Many investigations both theoretical and experimental, have been conducted for the flow about bodies in motion in an infinite fluid medium. These focused on the mechanism of flow separation and vortex shedding. Researchers in offshore structures and ship hydrodynamics have studied surface piercing bodies (Miyata & Inui , 1984). Some studies have also been made of horizontal circular cylinders placed below the free-surface. Both forces due to waves (Skotner *et al.* 1994) and due to steady motion (Miyata, 1990) have been studied. Miyata *et al.* showed that the drag on the cylinder decreased with decreasing depth-radius ratio. Estimates were made of wave making resistance of a submerged sphere both theoretically by Havelock (1917) and in more recent numerical work by Wu (1995). Rockwell *et al.* (1995) recently investigated the behavior of the separated wake of a circular cylinder in the presence of a free surface. This work demonstrated additional evidence of the metastable wake configurations that are demonstrated in the present work. Particle Image Velocimetry (PIV) measurements conducted at GALCIT on the wakes of a sphere, cylinder and airfoil in the presence of a free surface also conclusively demonstrated that a metastable jet of separated fluid occurs, and dominates the wake, for a variety of body shapes.

The purpose of the present experiments was to study the interaction of the turbulent wake of a bluff body with a free surface. The presence of an underwater wake causes free surface deformation and wave patterns. These patterns are interesting by themselves and also serve as an indication of what occurs in the wake below the surface. The introduction of an asymmetric boundary condition into a problem with axisymmetric geometry requires topological changes in the wake structure. These changes manifest themselves directly and indirectly. Direct evidence of the boundary condition is the deformation of the free surface and the wake itself. Indirect

evidence is seen in a macroscopic sense in the variation of the drag as the bluff body approaches the surface.

The circular disk was chosen as an appropriate bluff body for several reasons. The symmetric submerged wake of a circular disk has been the focus of studies by researchers over the years. There exist, therefore, baseline data for comparison. In addition, the fixed location of the separation line and the absence of end conditions reduces the intrinsic complexity of the flow. The Reynolds number (Re) is based on the diameter 'd' and the Froude number (Fr.) is based on the separation 'h' between the disk edge and the free surface level far upstream. The reference velocity used for both numbers is the free stream velocity U_∞ The Reynolds number ranges from 40,000 to 70,000 and the Froude number ranges from 0.058 to infinity. The nomenclature used in this discussion is shown in Figure 1-1.

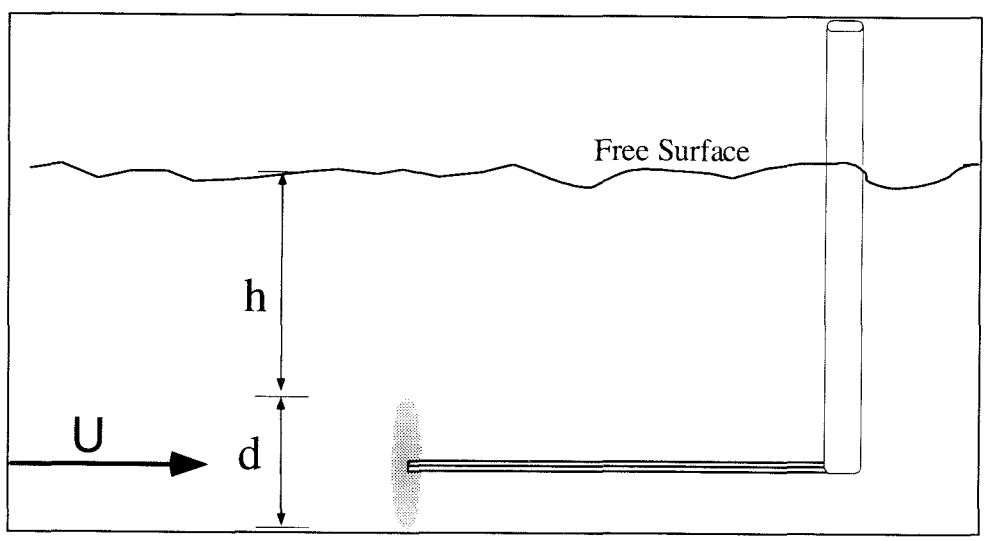

Figure 1-1 Nomenclature for disk experiments.

2. Experimental Apparatus and Procedure

2.1 Water Tunnel Facility

These experiments were conducted in the 'Noah' facility in the Guggenheim Laboratory basement. It is a low speed, free-surface water channel. A description of the facility as it was originally constructed and operated at the Jet Propulsion Laboratory (JPL) can be found in Gharib (1985). The test section of the facility is 18"x 22"x 60" and has glass walls and a glass floor. It is capable of stable speeds between 2 cm/s and 70 cm/s. For this experiment, the range of velocities used was between 30 cm/s and 60 cm/s. Gharib (1985) and Bridges (1993) report that the turbulence level in this facility was on the order of 0.1% or less. Spectrum analysis of the free stream velocity signal revealed no significant broadband noise characteristic of free-stream turbulence. These results indicate that the facility has a fairly low turbulence level.

A Laser Doppler Anemometer (LDV) was used to measure free-stream velocity. The LDV utilized a Spectra Physics 5 mW He-Ne laser (618 nm) and operated in a forward scatter mode. Detection was accomplished with a photodiode whose output was fed through a Dantec N55x frequency-counter tracker box. The resulting output voltage was scaled to account for fringe spacing and frequency and displayed as a velocity by the tracking box. The voltages were also output to an oscilloscope for visual confirmation of phase locking as well as to the A/D board of the computer-scope. The location of the sensing volume was at the tunnel centerline at a height of 10" from the bottom wall. The distance between the sensing volume and the sting was 18". A zero speed reference water level of 17" was used for all these experiments.

Since this work involves the presence of a free surface, it is prudent to discuss surface quality and cleanliness issues. For the range of velocities used in these experiments, there were small levels of surface deformation induced by the contraction and the test section walls. This

judgment is based on the relative amplitude of the surface disturbances generated by the facility to those generated by the model itself. It was decided to utilize standard Pasadena tap water, filtered for contaminants, to fill the tunnel. The surface was vacuumed each morning to remove dust and other large surface debris. No attempt was made to introduce or control the presence of surfactants. In other words, the surface was chosen to be uniformly and repeatably dirty.

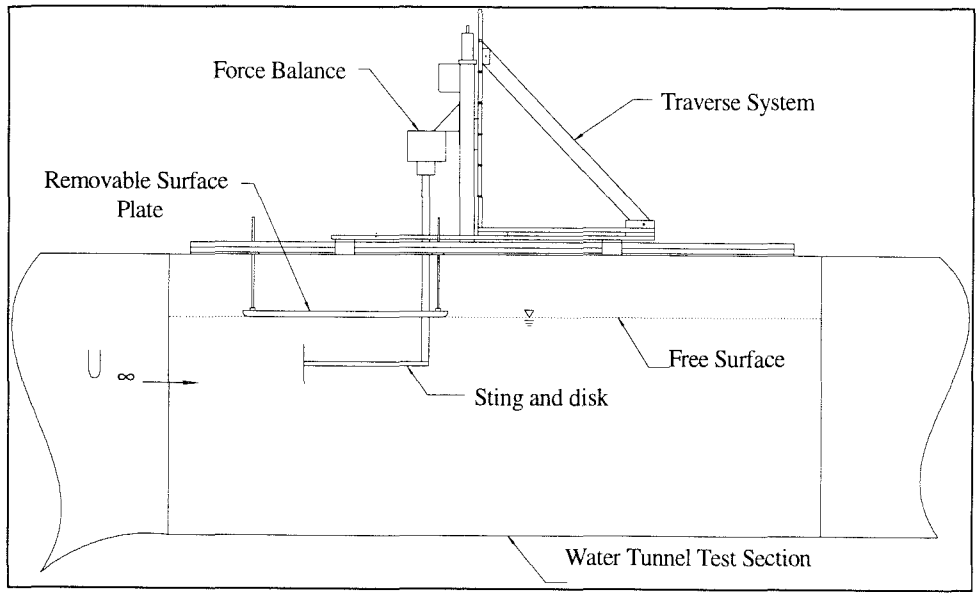

Figure 2-1 Schematic of the flow facility with the surface plate in place.

2.2 Traverse, Sting Support and Models

For the experiments performed for this thesis, convenient, repeatable and accurate positioning in the vertical (z) direction was necessary. To facilitate this a traverse was designed to sit atop the steel guide-rails on either side of the test section. The traverse is shown in Figure 2-1. The traverse was constructed to place the model between the tunnel walls and facilitate motion in the z direction. This was accomplished by utilizing a Compumotor traverse with 18" of travel aligned vertically as the model mounting platform. This traverse was controlled by an IBM-PC with a PC-23 controller card on board. This allowed programmable z motion. Positional

accuracy was ± 1 count, with 500,000 counts per inch of travel. The models were mounted at the end of a stainless steel sting which was constructed to cause minimum interference with the flow field. The sting consisted of a horizontal tube, 0.8 cm in diameter and 40 cm in length. This was attached to a vertical shaft which was an airfoil section to minimize drag. The tip of the horizontal tube was tapped with a 5-40 thread to enable a model to be screwed on. Both the vertical and the horizontal portions of the sting had graduated scales to help identify dimensions in images. The sting was mounted on the metric plane of a 3-component force balance and the balance mounted to the traverse's platform.

2.3 Drag Measurement

2.3.1 Force Balance

The force balance used was designed and built by Lisoski (1993). An excellent description of the balance and its accompanying amplifier along with engineering drawings, detailed calibration and utilization procedures may be found in the same reference. An average of many calibrations indicated a balance accuracy of about ±0.0005N. This equates to an uncertainty in measured force coefficients as:

$$\Delta C_d = \frac{\Delta F_d}{\frac{1}{2}\rho\, U_\infty^2 A} \equiv \frac{\Delta F_d}{\frac{1}{8}\pi\rho\nu^2 R_e^2}$$

This implies better resolution is obtained for larger Reynolds numbers. There are also uncertainties present in C_d due to uncertainties in the other quantities on the right-hand side.

A four channel force balance amplifier and power supply was designed specifically for use with this force balance. The data was acquired from the amplifier through an IBM-PC clone running an RC electronics 12 bit A/D data acquisition system. The 12 bit A/D converter gave a basic accuracy of 0.005 volts. Sampling rates varied from 64 to 256 μsec. Four channels of data

were recorded, these being N_1 , N_2, D and a voltage from the LDV corresponding to the flow velocity. The A/D converter has been calibrated to have a conversion accuracy of ±1 bit or 0.005V.

The force balance data was acquired for 32 seconds per data-point and the values of the force coefficients reported are averages over this period. The long measurement time ensured repeatability and reliability of the results. This corresponded in the worst case to 21 diameters of data and in the best case to 195 diameters of data.

2.3.2 Measurement Procedure

The force measurements were carried out for two disk diameters (3" & 4") and three velocities (40 cm/s, 50 cm/s & 60 cm/s). These correspond to a Reynolds number range of 25,000 to 65,000. For each of these cases, the disk was attached to the sting and lowered till the upper edge of the disk was just at the level of the free surface. At this point a reference zero level voltage reading was taken for the force balance. A second reference zero level reading was taken at the end of the experiment when the flow came to a stop. An average of these two zero levels was used as a baseline, by the analysis routines, to give the correct value of the force components.

The level of the water in the tunnel was then noted and the tunnel spooled up to the desired velocity as indicated by the LDV. The water level in the tunnel drops with increasing flow speed and therefore a correction to the height of the model is applied. This is done by lowering the model a distance equal to that by which the water level in the facility drops. This is taken as the reference position (h=0) for that particular run. When uniform flow has been established, the measurements are made. For the case of drag measurements, force-balance signals are collected for a period of 32 seconds on the computer scope and stored for further analysis. The model is then lowered to the next position of h/d and the procedure is repeated. For

completeness and for reasons of flow hysteresis patterns, readings were taken both while lowering the disk from the surface and while raising it again. A similar procedure is followed for all the disk diameters and velocities. For all the cases studied, both surfaces of the disk were fully wetted. In fact, due to surface deformation, the disk remains wetted for small negative values of h/d.

2.4 DPIV

Digital particle image velocimetry techniques were utilized to generate and analyze the velocity field in the wake of the disk. A detailed description of this technique is given in Willert (1991). This optical technique computes the velocity field by implementing a local spatial cross-correlation of two sequentially exposed particle images from a CCD camera. Particle images are generated by seeding the flow with fluorescent particles and illuminating a fine section of the flow with an argon ion laser sheet. The exposure time of each image and the delay between them are controlled by pulsing an electro-optic shutter mounted co-axially with the laser head. Images from the CCD camera were downloaded to a computer disk by means of an EPIX frame grabber. The image pairs were then analyzed by means of a proprietary DPIV code.

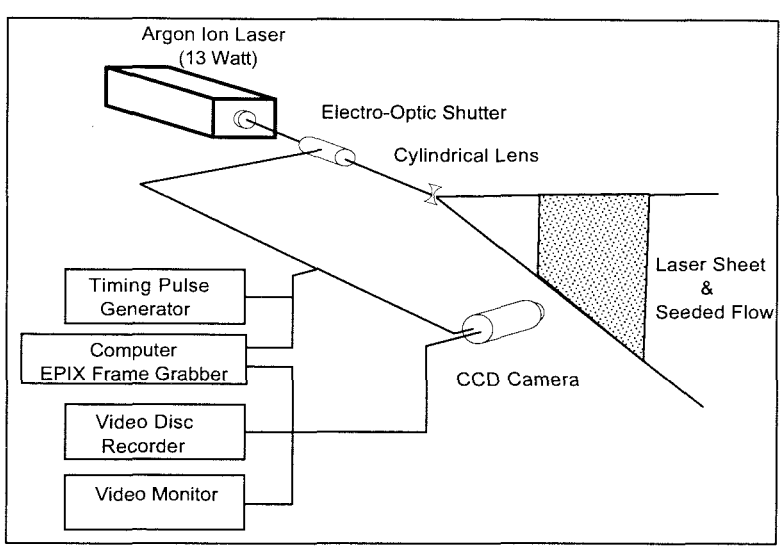

Figure 2-2 Schematic of the DPIV setup.

3. Free Surface Deformation

A principal point of interest in this study was the interaction of the wake of the submerged disk and the free surface. As the disk approaches the free surface from below it creates wave patterns on the surface. It was found that there were two distinct types of patterns present. These are hereafter referred to as the Mode-1 and Mode-2 patterns.

3.1 The Mode-1 Pattern

This is the surface deformation pattern that first appears when the disk is raised towards the surface from far below (Figure 3-1 & Figure 3-2). This is characterized by the presence of one or more bores on the surface behind the disk. The upstream flow forms a smooth standing wave over the disk and then plunges downward behind it forming a smooth depression on the surface as can be clearly seen in the underwater view. Two bores can be seen in Figure 3-1. The bore has the character of a breaking wave. Its steep upstream face is covered by a group of capillary waves and tiny bubbles which appear on the surface when the wave periodically breaks. The secondary bore appears behind the first one and has the same features as the first bore though they are less prominent. All the wavefronts are curved due to the local nature of the disturbance caused by the disk. The standing wave on the disk appears to be spatially steady. However, the bores tend to oscillate in the flow direction.

3.2 The Mode-2 Pattern

This is the pattern which appears to dominate when the disk is brought to small values of h/d ($h/d < 0.5$) by lowering it through the free surface. This is shown in Figure 3-3 & Figure 3-4. The flow is dominated by a bow wave that extends from the plane of the disk forward. The forward edge of this crest is lined by capillary waves. The wave drops smoothly and sharply

behind the plane of the disk forming a curved trough in the wake. The rear surface of the crest has a group of capillary waves present on it as can be clearly seen in the underwater view (Figure 3-4). The wake is a region of strongly recirculating flow as is indicated by the upstream migration of bubbles on the surface. The wave pattern in this mode appears to be spatially steady.

3.3 Hysteresis and Stability of Surface Patterns

It was found that the two patterns appear to have limited regions of stability. A disk that approaches the surface from below has an axisymmetric flow around it in the mean. However, at some point it becomes 'aware' of the presence of an asymmetric boundary condition in the form of a free surface. The flow first loses its axisymmetry and then makes a topological change to accommodate the new boundary condition. The point at which the presence of the surface is felt and the point where the wake adjusts for its presence, through a Mode-1 to Mode-2 transition, are not the same. The same argument is true for a disk being lowered away from the free surface. At some point the flow loses its 'memory' of the surface boundary condition and transitions back to Mode-1 topology. The interesting feature of this flow is that the h/d value at which the Mode-2 to Mode-1 transition occurs, is significantly different from that for the Mode-1 to Mode-2 transition. This difference, termed 'hysteresis', will be discussed further in the context of other measurements and observations.

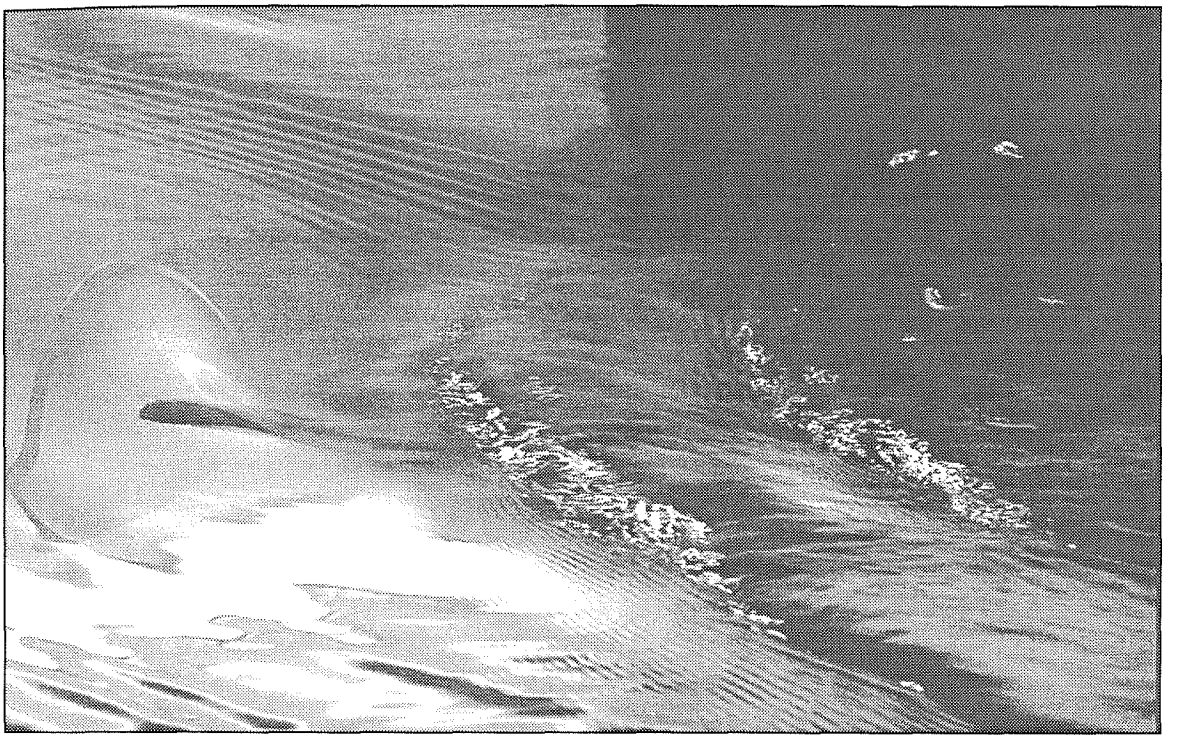

Figure 3-1 Mode-1 surface clearly showing two bores and capillary waves ahead of them. Flow is from left to right.

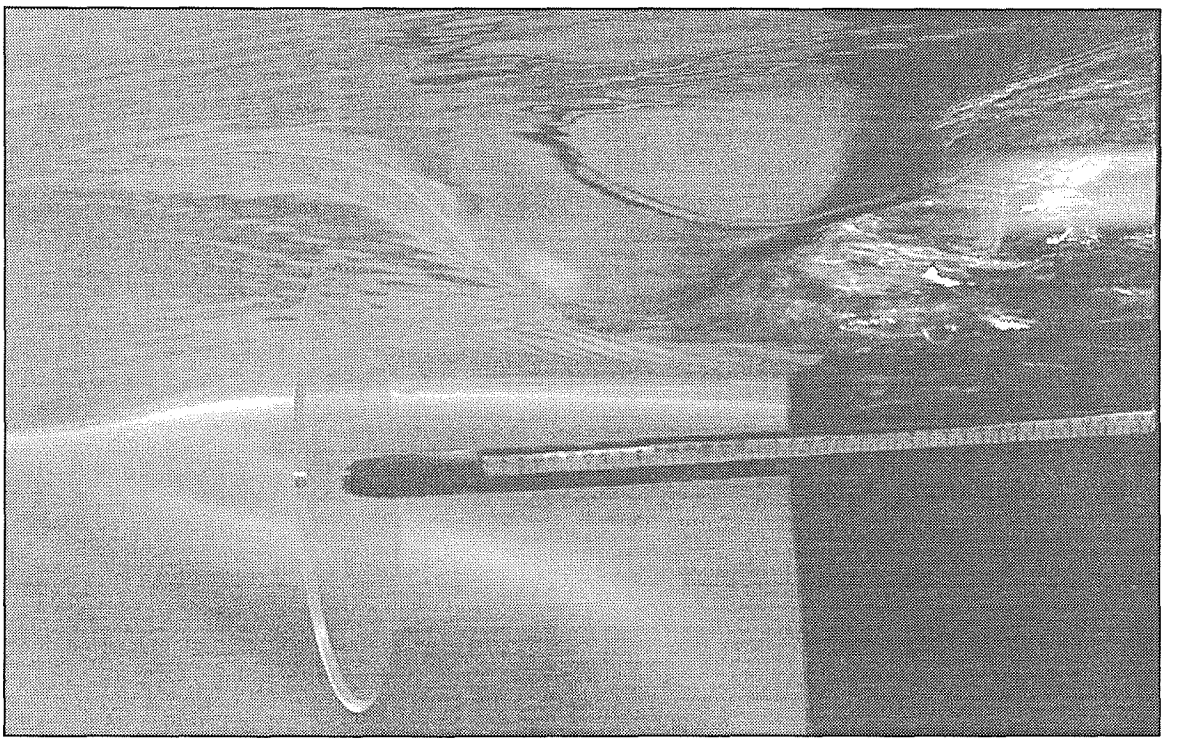

Figure 3-2 Underwater view of Mode-1 surface. Note depressed surface ahead of bore.

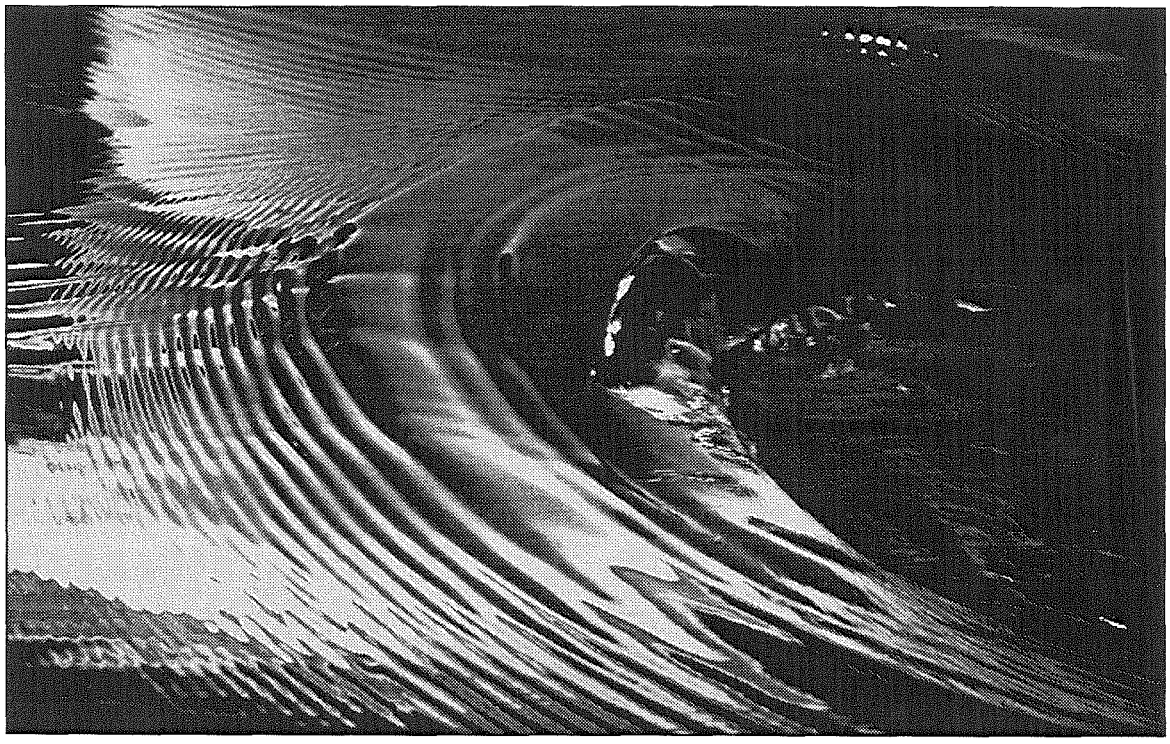

Figure 3-3 Mode-2 wave pattern showing bow wave above the disk with a steady pattern of capillary waves ahead of it. Also note the steep drop into the wake at the rear of the disk and the air bubbles being entrained there. Flow is from left to right.

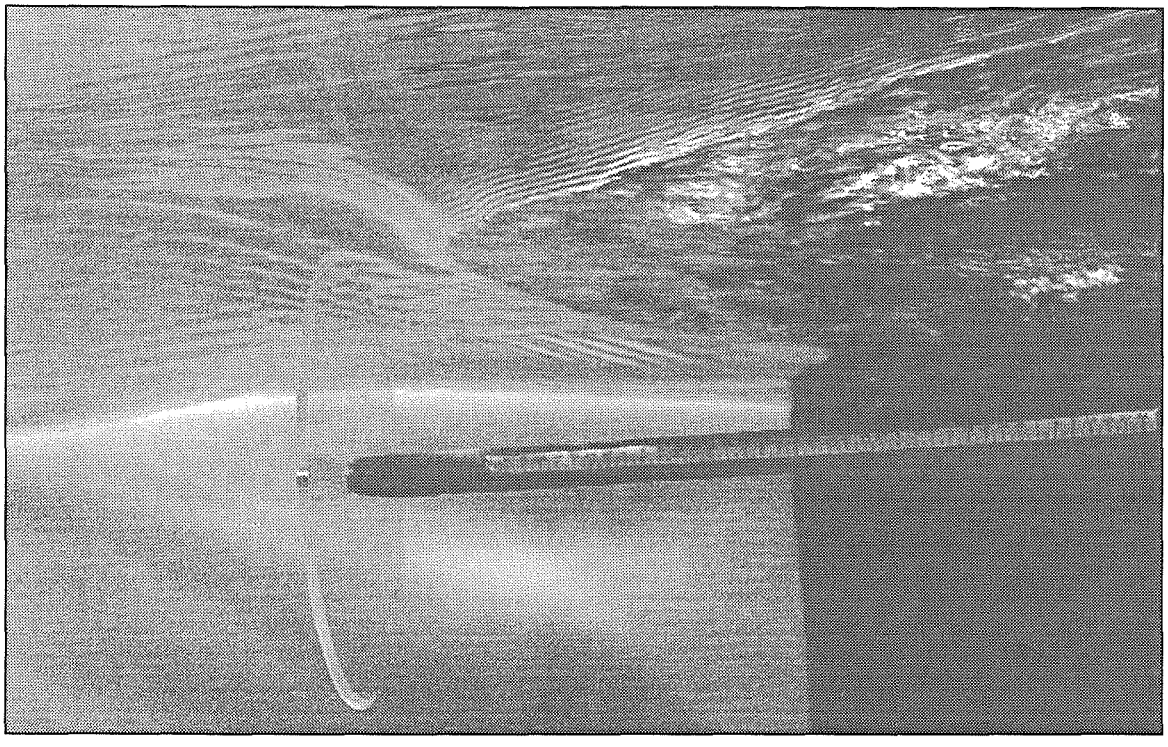

Figure 3-4 Underwater view of Mode-2 surface. Note the curved shape of the depressed wake region with capillary waves on its forward face.

3.4 Air Entrainment and Surface Broaching

The entrainment of air into the wake is evidenced by the presence of air bubbles behind the disk. In Mode-2 flow, there appears in the wake a bound horseshoe vortex, the upstream edge of which lies behind the upper edge of the disk. The vortex is steady in space and time and is not shed periodically. The core of this vortex is made visible by the entrainment of air (Figure 3-5).

Usually in non cavitating flows, air is entrained along the core of vortex connected to the surface. However, in this flow, air is entrained along the length of a contact line which forms along the interface between the downward flow at the rear of the disk and the upstream flow in the recirculating region. Both surfaces have positive curvature at the contact line and form a cusp that permits entrainment of air into the flow as shown in Figure 3-6 and Figure 5-8.

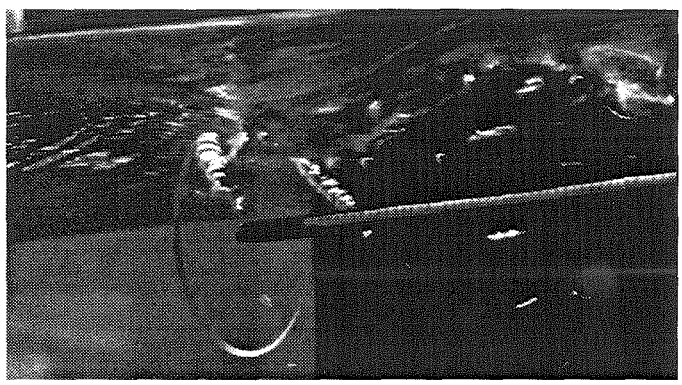

Figure 3-5 Mode-2 bound vortex creating a bubble trail.

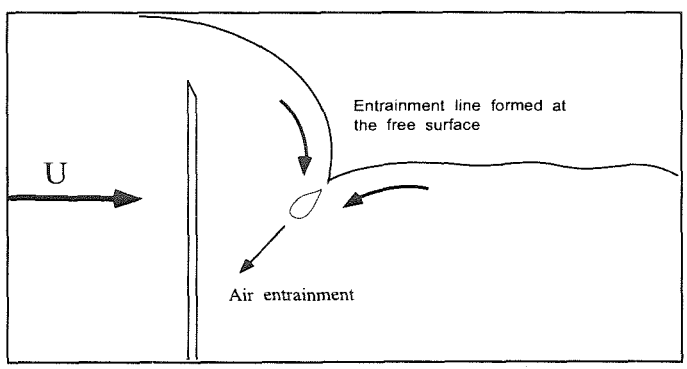

Figure 3-6 Schematic of air entrainment in Mode-2 flow through the formation of a surface cusp.

4. Results of Drag Measurements

4.1 Free Surface Boundary Condition

The results presented here are not corrected for blockage. This is for two reasons. The first is the fact that the effect of blockage in the presence of the free surface is not very clear. Secondly, blockage corrections for three dimensional bodies are not well understood and appear to be highly empirical at best. What is important in the present work are the trends that the data exhibit and their relative magnitude. The absolute values are not of critical importance to the conclusions. Therefore, all drag coefficients presented here are normalized to the fully submerged value. The measured Cd for the fully submerged 4" dia. disk (4.2% blockage) was 1.3, which is higher than the value of 1.15 - 1.2 reported in the literature (Blevins 1984).

Figure 4-1 shows the drag of the sting alone and that of a sting with a 4" dia. disk suspended 0.2" ahead of it to simulate the shielding effect in the actual measurements. For comparison the drag of 4" dia. disk at the same velocity is 1.75 N. Sting drag is seen to be a negligible fraction of the total measured drag. Therefore, the results presented here are not corrected for sting drag.

The normalized drag coefficient for a disk approaching a free surface is plotted for various values of h/d as shown in Figure 4-2. It may be seen that Cd increases with decreasing h/d to a maximum value before decreasing again. This maximum occurs at an h/d ~ 0.075 $\pm$ 0.025. The uncertainty in the absolute value of h/d arises from the fact that the free surface height varies by $\pm$ 0.1" due to sloshing.

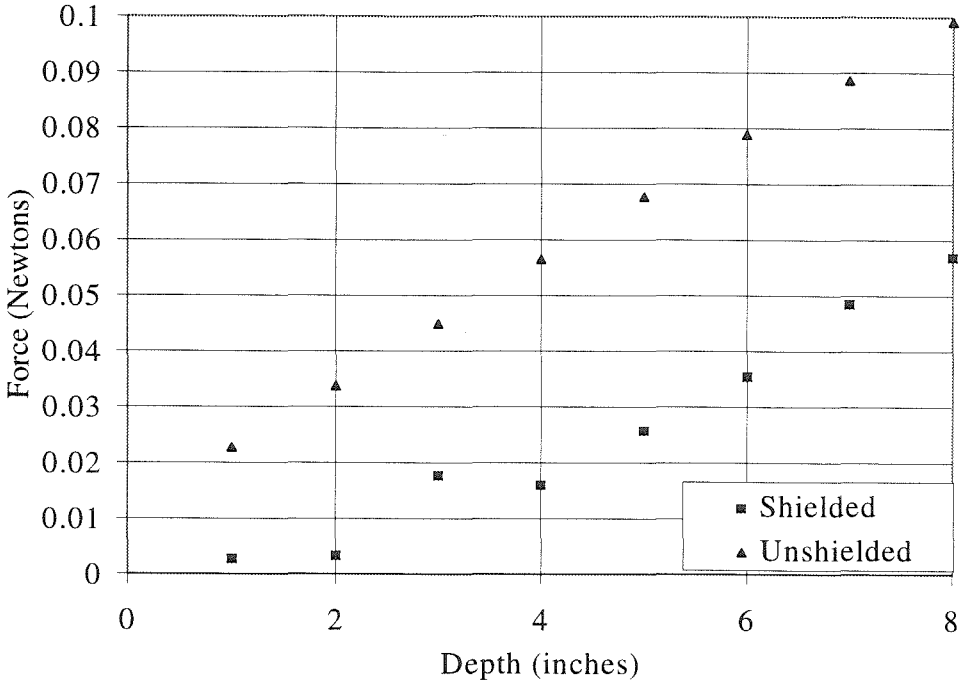

Figure 4-1 Graph showing sting drag at $U_\infty = 60$ cm/s.

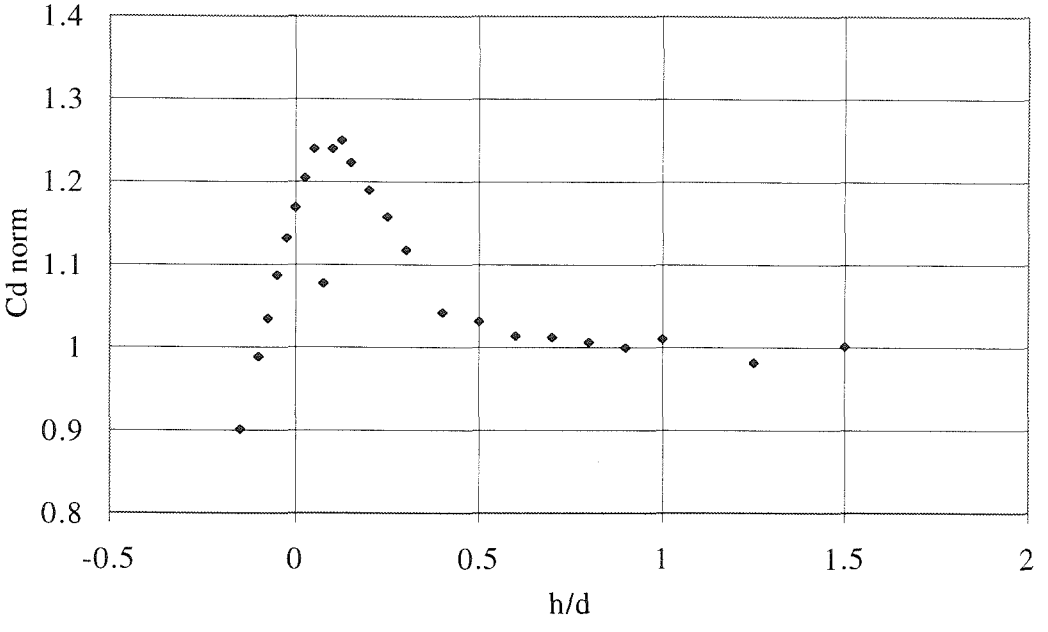

Figure 4-2 Variation of normalized drag coefficient with h/d ($U_\infty = 60$ cm/s, d = 4").

Similar measurements were made for disks of 3" (7.62 cm) and 4" (10.16 cm) diameter at velocities in the range of 40 cm/s to 60 cm/s. These are shown in Figure 4-4, Figure 4-5 and Figure 4-6. It was found that peak height varied with U_∞. From the figures it may be seen that the maximum peak height at 50 cm/s is slightly greater than that at 60 cm/s and roughly twice that at 40 cm/s. For U_∞<40 cm/s the magnitude of the peak progressively diminished to the point where it was indistinguishable from experimental scatter.

The Froude number Fr. based is also plotted in Figure 4-7. It may be seen that the peak in the drag curve occurs at approximately the point at which Fr. = 1.

At some flow velocities and values of h/d, flow induced vibration of the sting support was present. This is to be expected since the disk is mounted on a cantilevered support with its own natural frequency of vibration. A spectral analysis of the drag traces as well as the natural response of the sting indicated that there was a strong overlap at 7.5 Hz as well as lesser overlap at other frequencies. The effect of this is a measured Cd that is lower than would be expected from neighboring points. The low Cd value indicated at h/d = 0.075 in Figure 4-2 is such a point. These points are included for completeness. Though they do not represent the expected value of Cd for the corresponding value of h/d, their low value is not due to experimental error but due to a fundamental change in the properties of the wake for that particular measurement. This point will be explained in detail in later discussions.

4.2 No Slip Boundary Condition

The free surface boundary condition is not a precise one. Even though the pressure along it is constant, it deforms and therefore the effect it has on the disk changes too. The surface wave patterns serve to radiate energy away from the body and provide a contribution to the measured drag. Since the free surface wave pattern is complex, no simple analysis is possible to estimate

the energy radiated into the far field by the surface displacement. It was therefore decided that a simpler way to estimate the effect of wave making on the drag would be to suppress surface deformation entirely. This is achieved by the introduction of a non deformable boundary in the form of a plate touching the free surface (Figure 2-1). A short surface-plate was used as this did not have the added complication of boundary layer build up. The disk was located 20 cm from the edge of the plate and therefore encountered a boundary layer of 0.45 cm thickness at the lowest Reynolds number.

It may be seen from Figure 4-3 that the disk suffers a rise and fall in drag when approaching a solid boundary. However, the magnitude of the increase is about 25% of that experienced near a free surface. In addition the location of the peak appears to have shifted towards lower values of h/d (h/d ~ 0.05) where h is the distance from the upper edge of the disk to the plate. In all the measurements, there appears to be a secondary peak of much smaller magnitude around h/d = 0.5.

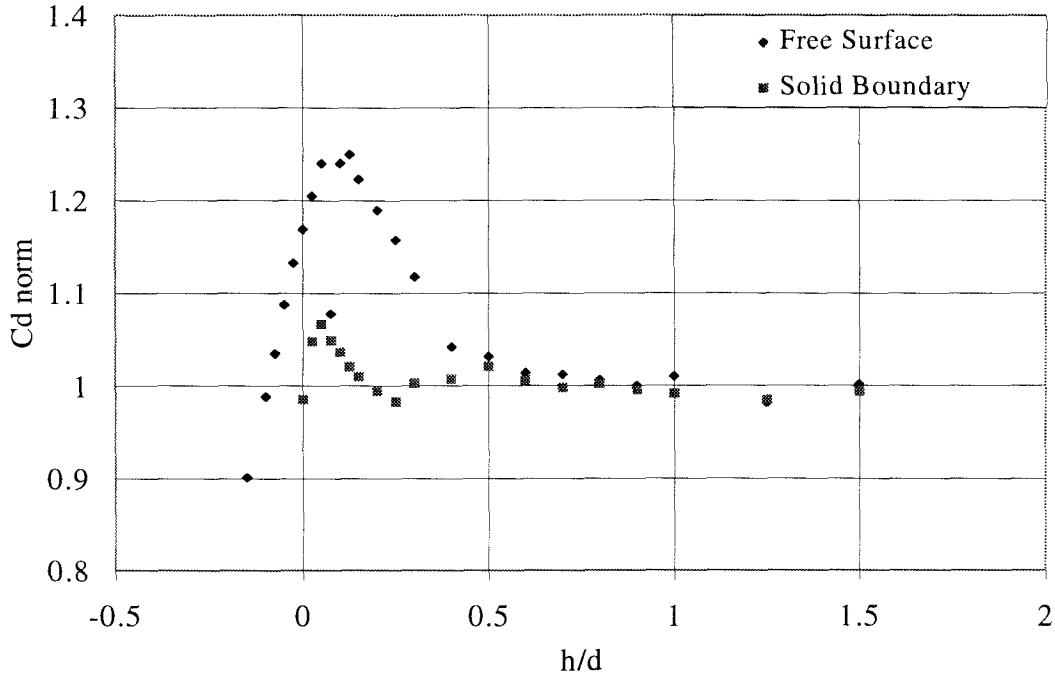

Figure 4-3 Comparison of the effect of a solid boundary versus a free surface on the drag of a circular disk (U_∞ = 60 cm/s , d = 4").

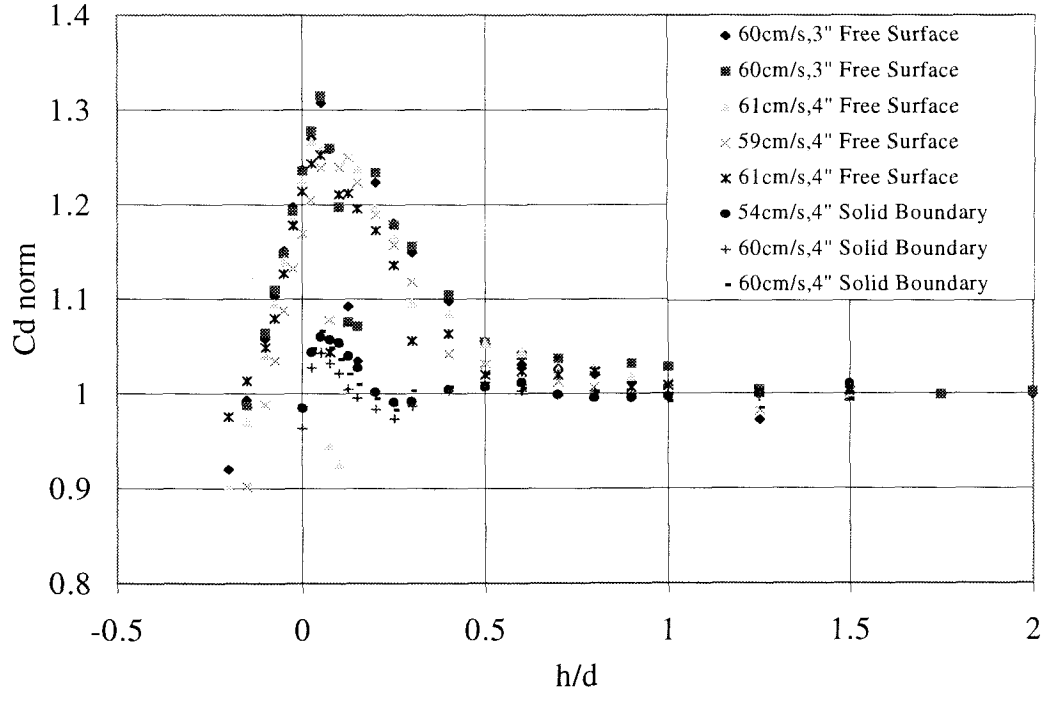

Figure 4-4 Summary of drag data at U_∞ = 60 cm/s.

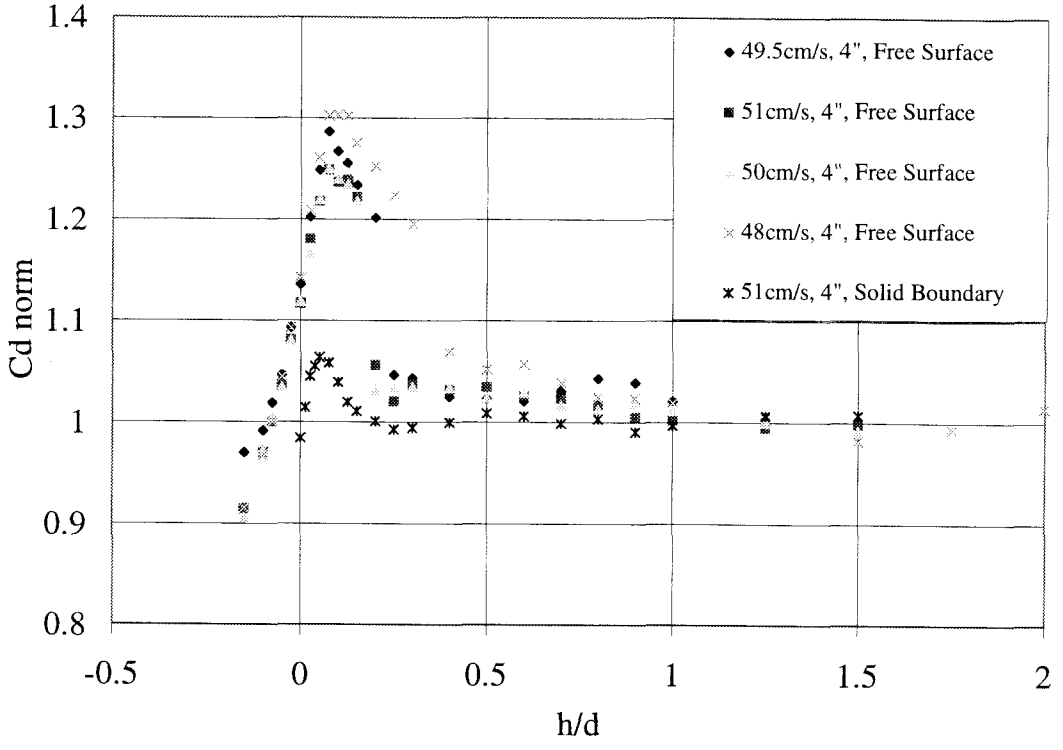

Figure 4-5 Summary of drag data at U_∞ = 50 cm/s.

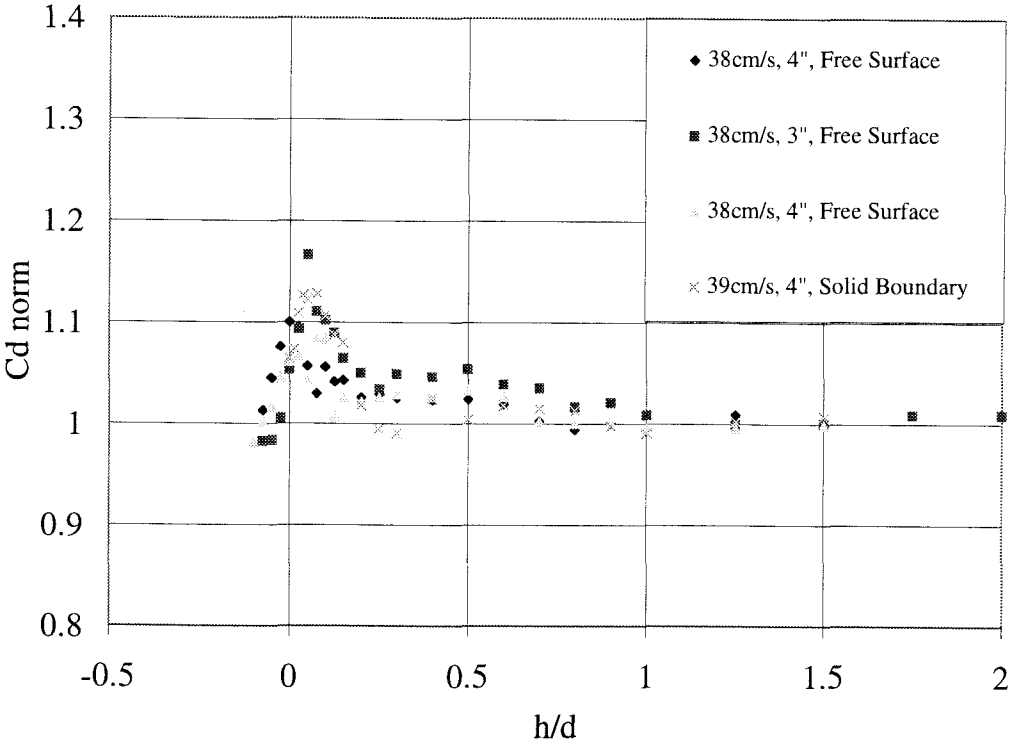

Figure 4-6 Summary of drag data at U_∞ = 40 cm/s.

4.3 Transition and Hysteresis in Drag Measurements

It may be observed that while the points in Figure 4-4 fall on a smooth curve, those in Figure 4-5 seem to have a discontinuity at h/d = 0.2. It was first believed that this was an artifact of the measurement, perhaps due to a missing measurement on the relatively steep slope. This is possible since the ± 0.1" oscillation of the free surface makes an accurate determination of h difficult. To further study the behavior at this point, another measurement was made for the case of a 4" diameter disk at 50 cm/s. This measurement was made for a full cycle of raising the disk in steps to the surface, from 3 diameters below, to the point at which the disk edge penetrated the surface and then lowering it again to its fully submerged condition. The results from this measurement exhibit an unusual feature as shown in Figure 4-7. It may be seen that while raising the disk there is a sharp jump in drag of about 20% at h/d = 0.2 and then a smooth increase to a peak value of +25% before decreasing as it approaches the surface. However, when the disk is lowered through the surface, the drag follows a smooth curve characteristic of measurements at the higher velocities. Therefore, there is evidently a significant difference in the properties of the wake when the disk is being raised compared to when it is being lowered.

A second significant feature exhibited by this plot is the difference in the value of h at which the nominal drag condition can establish itself. On the way up this condition exists till the disk reaches a depth of h/d = 0.2 before the sharp increase occurs. However, the disk has to be lowered all the way to h/d = 0.5 on the way down to restore the nominal value. This difference in h/d is a quantitative expression of the hysteresis phenomena. Figure 4-7 also shows the Froude number. The fact that the drag peaks at Fr. ~ 1 is consistent with theoretical (Havelock, 1917) and numerical studies (Scullen and Tuck, 1995) of the wave resistance on submerged bodies in potential flow.

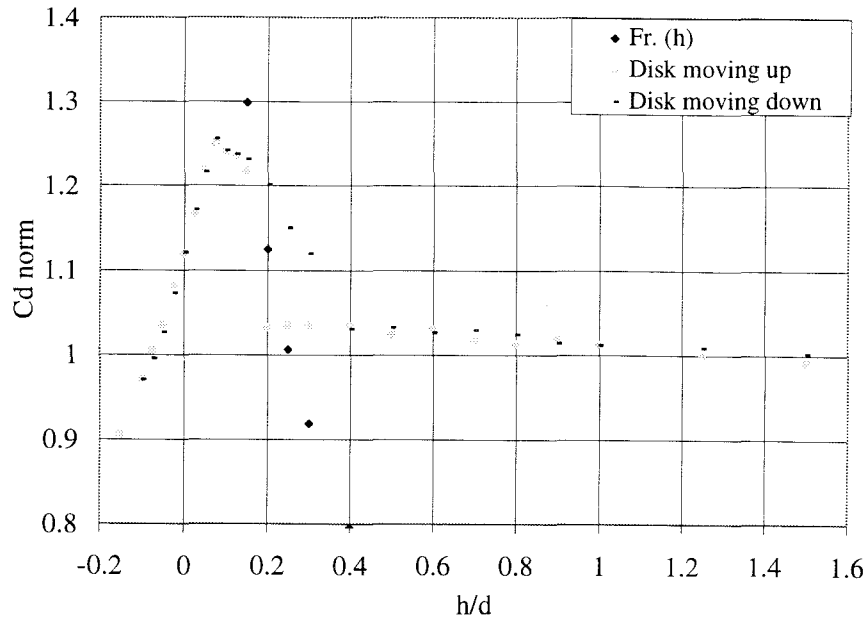

Figure 4-7 Hysteresis behavior in drag measurement

An issue of interest here is the speed at which this increase in drag occurs. An examination of the drag traces indicated that this is a very fast transition. A sample trace from the force balance (Figure 4-8) shows that the rise in drag takes 0.25 sec or less, a flow time-scale of 2 to 3 diameters. This plot clearly shows that the wake is changing from a state of low drag to a state of higher drag. The precise nature of this transition is made clear in the next section.

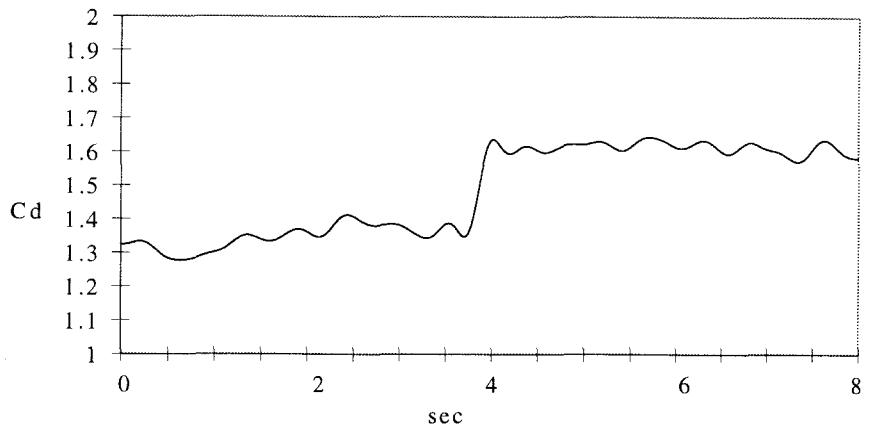

Figure 4-8 Drag rise during Mode-1 to Mode-2 transition

5. Flow Visualization

5.1 Results

Flow visualization was performed by illuminating the flow from below with a laser sheet aligned with the flow and normal to the surface. The sheet was offset by 0.4 cm from the centerline to allow for the presence of the sting. The flow was seeded with fluorescent particles. Particle streak images were obtained by increasing the exposure time of the CCD camera to the point where the particles had appreciable movement during the exposure. The resulting streak patterns are shown in Figure 5-1 to Figure 5-15. These represent a series of photographs taken with the disk first approaching the free surface (decreasing h/d) from below and then being lowered again. Flow is from left to right. Upward and downward movement of the disk are denoted by (↑) and (↓) respectively. The mode patterns are indicated by M1 (Mode-1) and M2 (Mode-2). The photographs were taken through the side wall of the tunnel viewing the disk at slight upward angle. This was necessary in order to be able to see the surface despite its transverse curvature. Features like the bores in Mode-1 flow cannot be clearly seen because of extreme curvature. These features can be inferred by the pattern of the surrounding flow. The hazy uniformly gray region at the top of each picture is the free surface. Since the surface is reflective, this region exhibits some weak streaks which should not be confused with the actual flow. The slightly sloping white line just below the top edge of the images is the relatively undisturbed free surface as it touches the tunnel side wall.

This series of photographs reveals some remarkable behavior in the wake. In Figure 5-1 it may be seen that the wake already shows some differences from the wake of a fully submerged disk. The flow approaching the top of the disk separates at the disk edge and the resultant shear

layer is deflected downward due to the presence of the free surface. An interesting feature that is evident in this image, is that the fluid separating from the top edge of the disk forms a jet that stays attached to the surface (Figures 5-1 t0 5-3). This high speed stream develops into the bore that is characteristic of Mode-1 flow. The jet of fluid bends upwards at the bore, is deflected downward by the rear face of the bore and is injected into the recirculating flow behind the disk, as can be clearly seen in Figure 5-4. The bore oscillates in the streamwise direction about some mean position which moves closer to the disk as h/d is reduced. Several other effects are noticeable as h/d is reduced: the free surface curvature at the rear of the increases; the bore becomes steeper and the downwash from the bore becomes more pronounced. All these features may been seen in Figure 5-5 which represents a Mode-1 flow at h/d = 0.05.

If the flow is left standing at this value of h/d, it undergoes a sudden transition to a wake with entirely different structure. There occurs a rapid detachment of the jet from the free surface and reattachment to the rear of the disk as can be seen in Figure 5-6. This high speed jet of fluid now flows along the rear of the disk and joins the lower shear layer. This has the effect of converting the wake behind the jet into a single region which recirculates anticlockwise. The jet at the top of disk is vectored along the free stream direction. In the process of attaching to the disk, it has to curve sharply downward. This curvature has to be balanced by a pressure gradient which results in a low pressure recirculating region just behind the top edge of the disk (Figure 5-6). This recirculating region is the location of the core of the bound horseshoe vortex mentioned in the context of air entrainment. In Figure 5-7 an air bubble can be seen trapped in this region. The associated low pressure contributes to increased drag. Also visible in Figure 5-7 and Figure 5-8 is the surface cusp formed at the entrainment contact line. These observations may be correlated with the discussion on the Mode-1 to Mode-2 transition in Section 3 and Section 4. Further reduction in h/d results in the jet being pinched off, resulting in weaker recirculation in the wake.

When the disk is lowered (increasing h/d), as shown in Figures 5-9 to 5-15, the evolution of the wake topology is different from that when the disk is being raised. The most prominent difference is that instead of reattaching itself to the free surface at h/d = 0.05, the jet is now able to penetrate the wake at all angles between the disk and the surface. As h/d increases, the size of the recirculating region just behind the disk grows (Figures 5-10 and 5-11) as does the thickness of the jet that forms it. As this recirculating region grows with increasing h/d, the jet is deflected into the wake at increasingly shallow angles with respect to the free surface. Figure 5-14 shows the wake in Mode-2 flow at h/d = 0.25. At this h/d, the wake undergoes a reverse transition by attaching the jet to the free surface, re-establishing Mode-1 flow (Figure 5-15).

The difference in the h/d values for the forward transition from Mode-1 to Mode-2 (h/d = 0.05, Figure 5-6) and reverse transition from Mode-2 to Mode-1(h/d = 0.25, Figure 5-15) is the basis of the hysteresis argument.

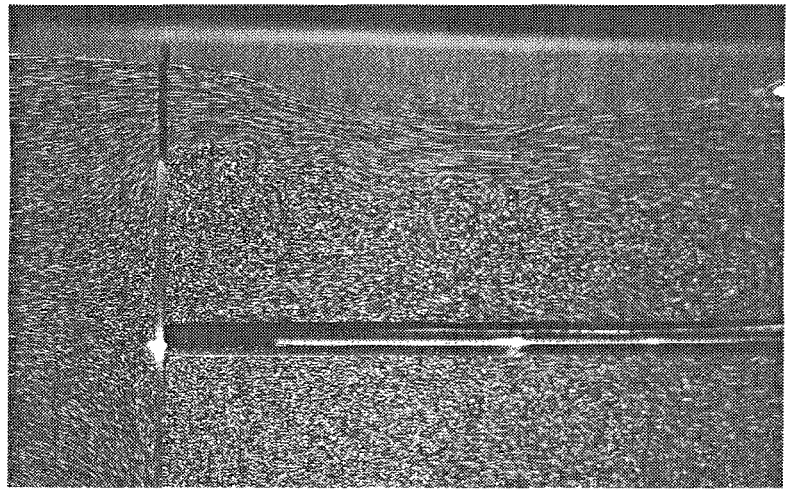

Figure 5-1 M1 (↑), h/d = 0.25, h = 1".

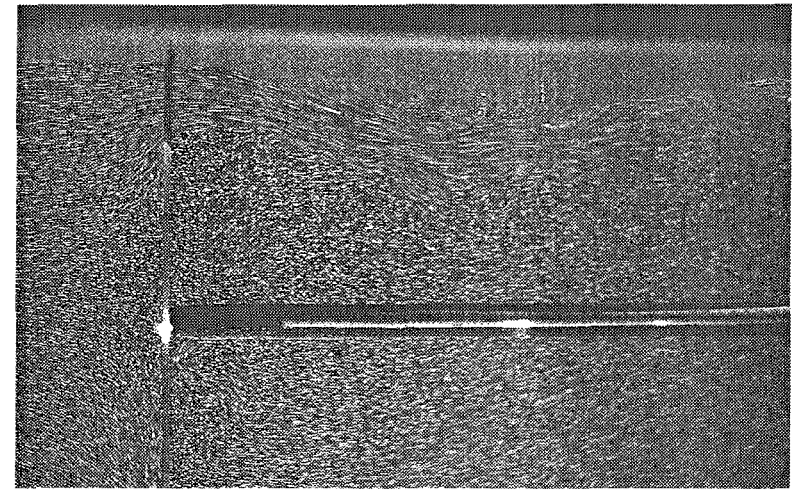

Figure 5-2 M1 (↑), h/d = 0.2, h = 0.8".

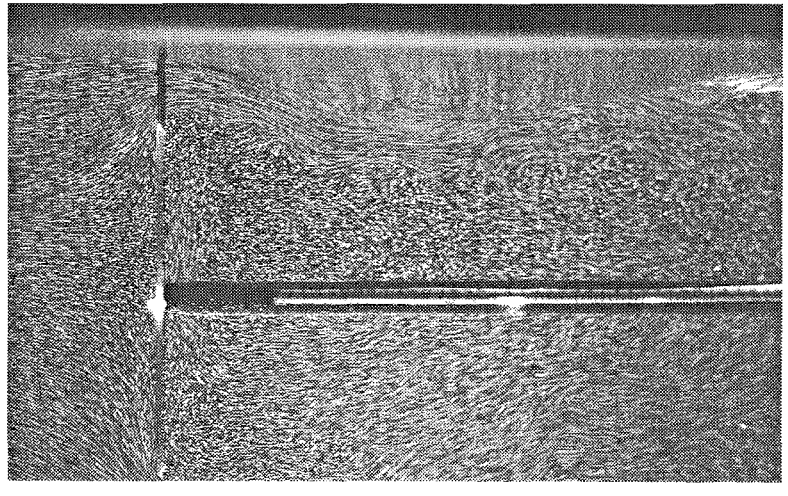

Figure 5-3 M1 (↑), h/d = 0.15, h = 0.6".

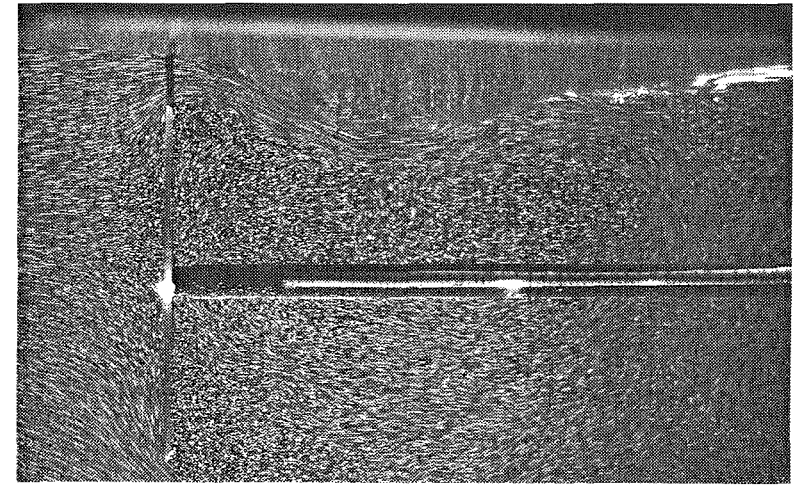

Figure 5-4 M1 (↑), h/d = 0.1, h = 0.4".

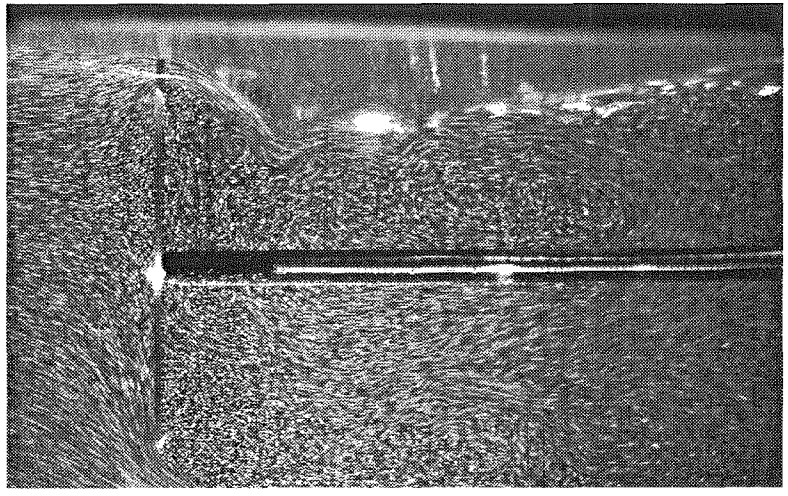

Figure 5-5 M1 (↑), h/d = 0.05, h = 0.2".

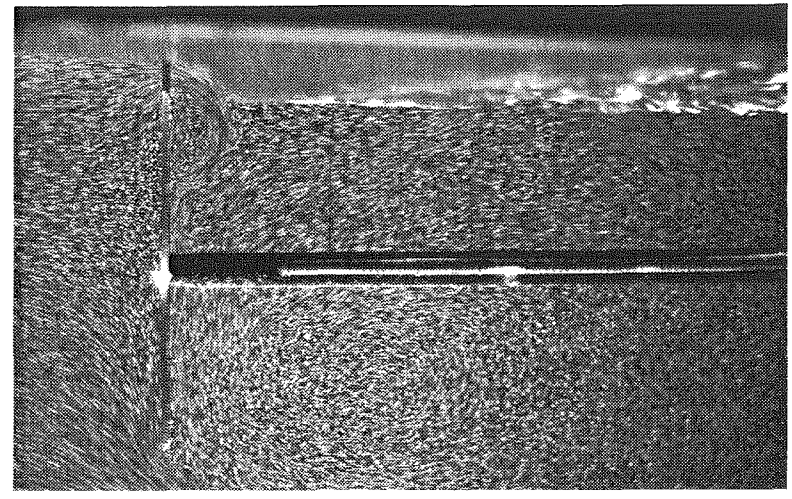

Figure 5-6 M2 (↑), h/d = 0.05, h = 0.2".

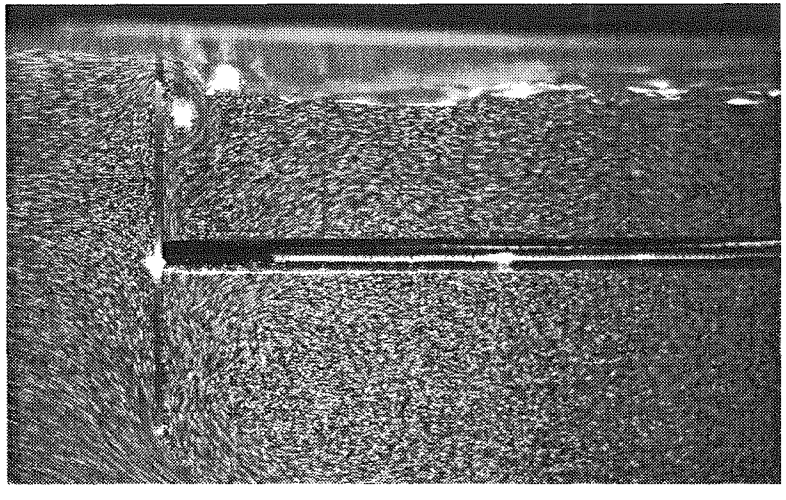

Figure 5-7 M2 (↑), h/d = 0.025, h = 0.1".

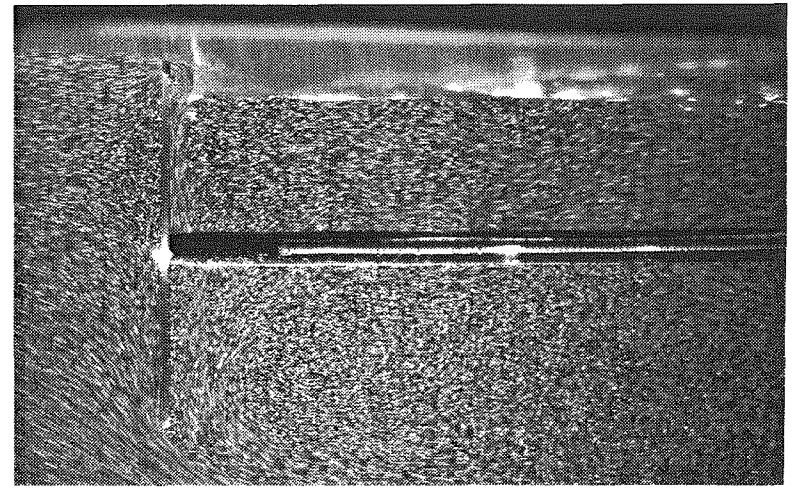

Figure 5-8 M2 (↑), h/d = 0, h = 0".

25

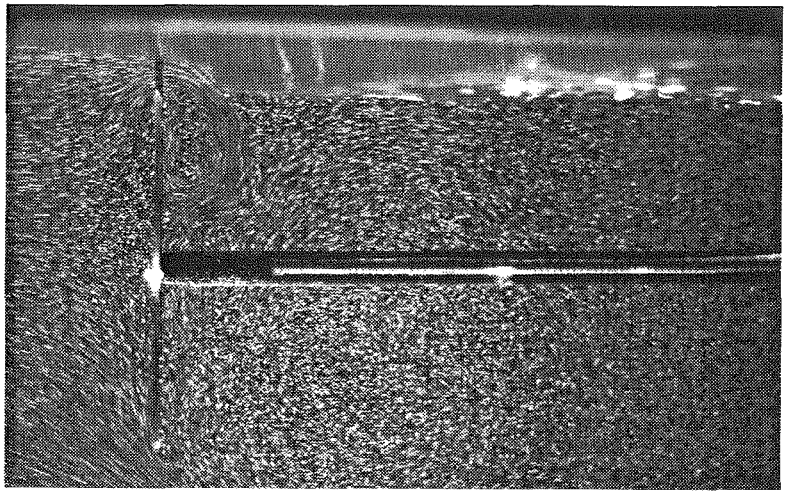

Figure 5-9 M2 (↓), h/d = 0.05, h = 0.2".

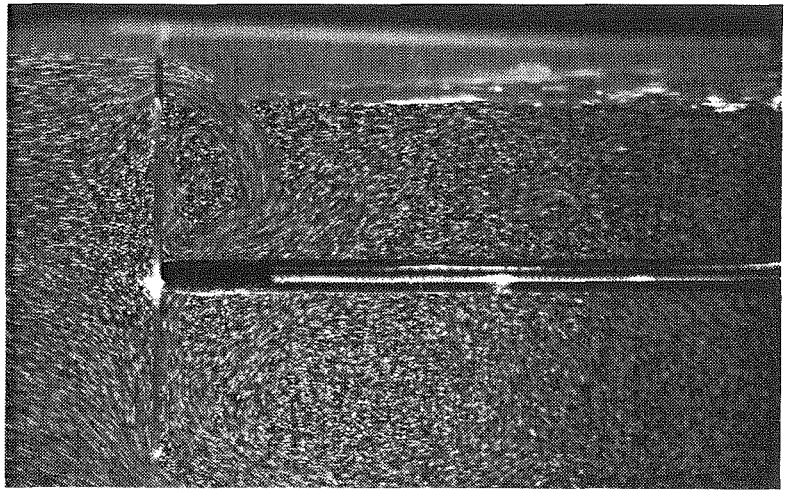

Figure 5-10 M2 (↓), h/d = 0.075, h = 0.3".

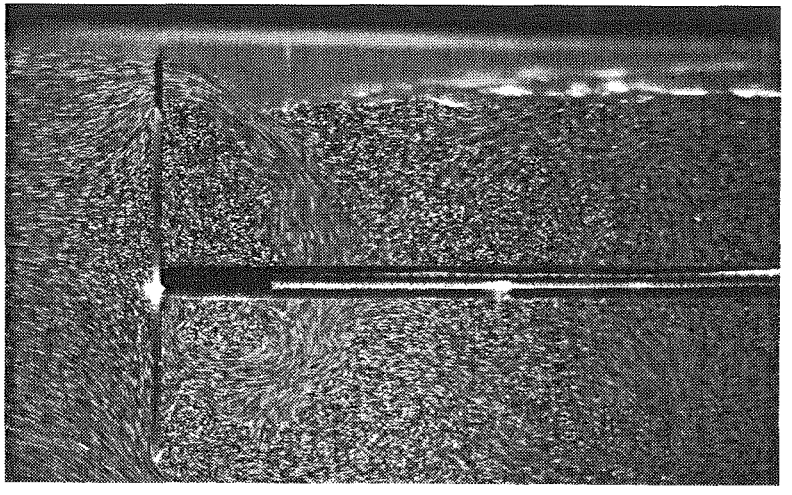

Figure 5-11 M2 (↓), h/d = 0.1, h = 0.4".

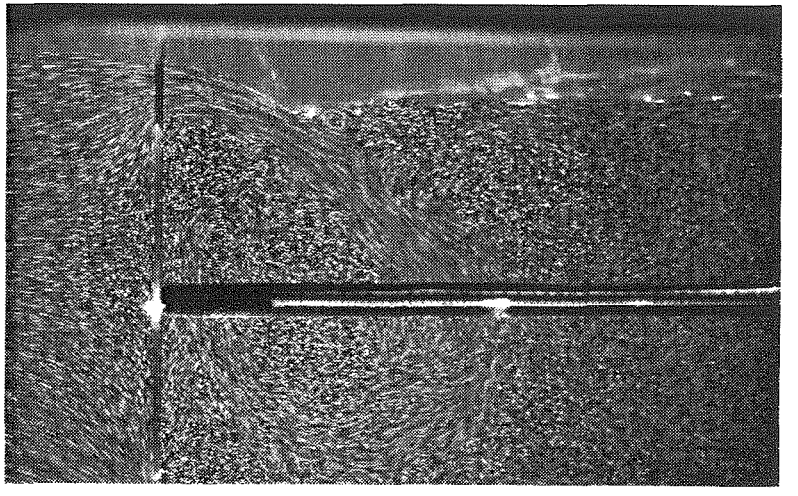

Figure 5-12 M2 (↓), h/d = 0.15, h = 0.6".

26

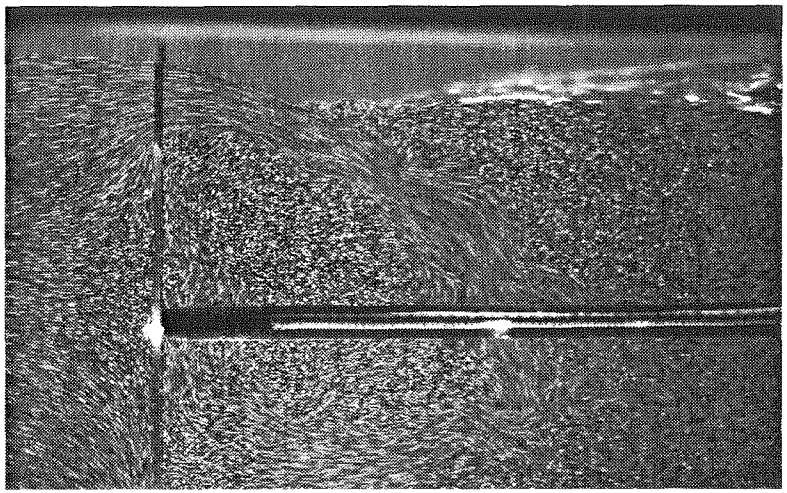

Figure 5-13 M2 (↓), h/d = 0.2, h = 0.8".

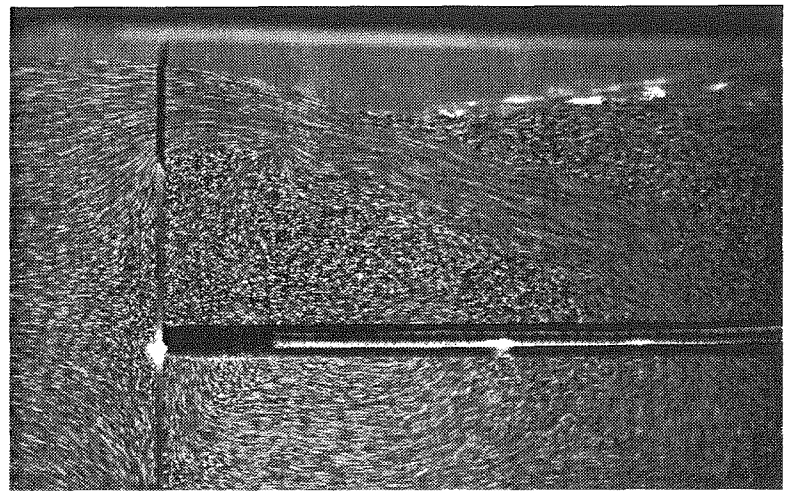

Figure 5-14 M2 (↓), h/d = 0.25, h = 1".

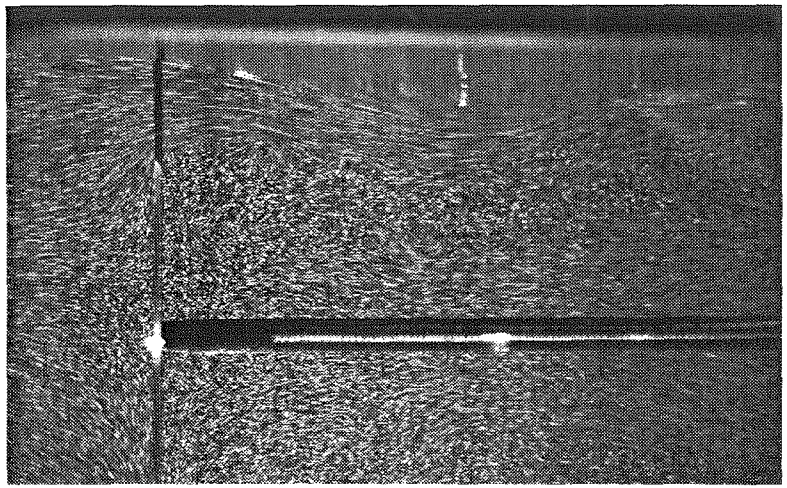

Figure 5-15 M1 (↓), h/d = 0.25, h = 1".

27

5.2 Discussion

Two flow states clearly exist and these are referred to as Mode-1 and Mode-2. They have distinctive features that distinguish them. The discussion above demonstrates how the flow switches between these two modes. A sketch of the symmetry-plane streamlines is shown in the figure below. The mean-flow streamlines for Mode-1 flow are the same as that for a disk in an infinite medium with a recirculating near wake. The symmetric form of the wake first deforms due to the approaching free surface before it undergoes a transition to the Mode-2 wake. It is hypothesized in Mode-2 flow, that there is a recirculating region with outflow adjacent to the free surface. If this outflow were not present, then the separatrix nearest to the surface would merge with it giving a simple recirculating region.

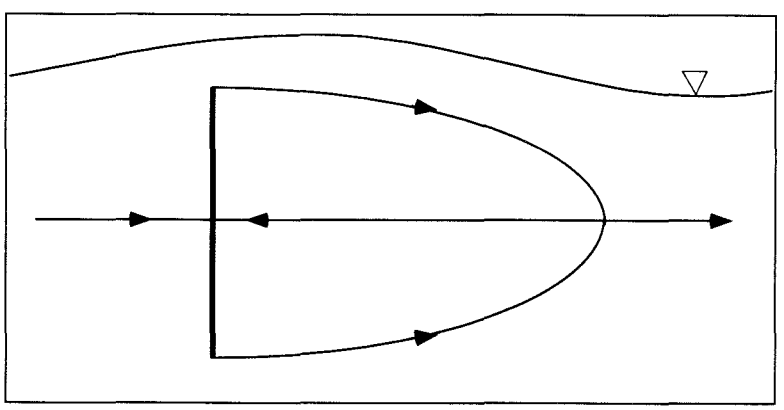

Figure 5-16 Mode-1 Symmetry-Plane Streamlines.

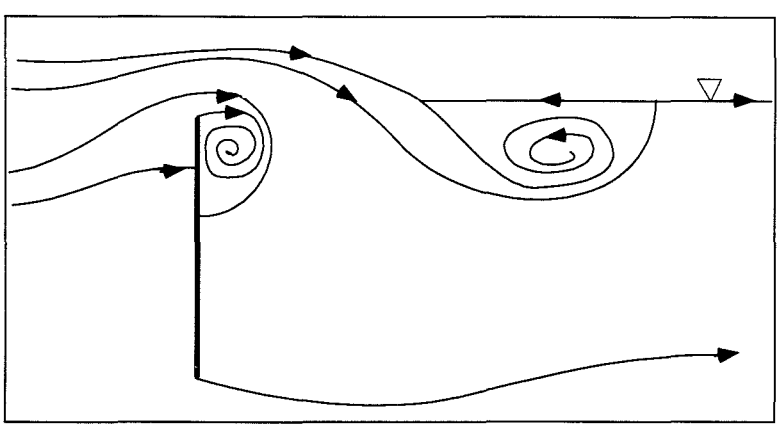

Figure 5-17 Mode-2 Symmetry-Plane Streamlines.

5.2.1 Transitions

The three velocity groups studied indicate three different categories of transitions between the two modes. These are the sudden, progressive and random transitions.

5.2.1.1 Sudden Transition

The transition described in Section 5.1 is called the sudden transition. This definition is based on the time-scale on which the mode switching occurs. The discontinuity at h/d = 0.2 in Figure 4-5 is caused by such a transition. The wake exists in a different mode on either side of this discontinuity. Sudden transitions are observed only from Mode-1 to Mode-2.

5.2.1.2 Progressive Transition

The drag curves at 60 cm/s (Figure 4-4), were found to be smooth irrespective of the direction in which a particular h/d value was reached. The reason behind this is what is termed progressive transition. In this case, for decreasing h/d, the jet smoothly detaches from the surface and manages to hold intermediate angles in the wake before finally attaching itself to the rear of the disk. It also exhibits similar behavior for increasing h/d. This does not mean that mode switching is absent. Mode switching occurs at a larger value of h/d ~ 1, resulting in Mode-2 flow over much of the h/d range.

5.2.1.3 Random Transition

An inspection of the curves at 40 cm/s (Figure 4-6) indicate that they are more irregular than those in Figure 4-4 and Figure 4-5. This behavior can now be understood in terms of the random transition. At this velocity, there appears to be random switching between the two modes. This is undoubtedly influenced by the noise level in the flow, but this is a factor that is not predetermined or steady. This dependence is highlighted by the fact that if the flow is susceptible to transition at a particular combination of U_∞ and h/d, the actual time it takes for the transition to initiate itself varies greatly, though the time for the transition itself to occur is fairly

consistent. In addition, laboratory observations indicated that time for initiation was less at higher velocities. Figure 5-18 shows the three types of transitions. A Mode-1 to Mode-2 sudden transition occurs at ~ 7 sec, a Mode-2 to Mode-1 progressive transition at ~ 18 sec and they jointly represent a random transition for this fixed value of h/d and U_∞ .

The occurrence of the sudden transition is also the reason for the low Cd value at h/d = 0.075 in Figure 4-2. The vibration of the sting in the horizontal plane induces a random transition in the wake. Since the result reported is an average over 32 seconds, it appears as a value between the two states. If shorter sections of the same traces are examined, they yield values corresponding to the component modes.

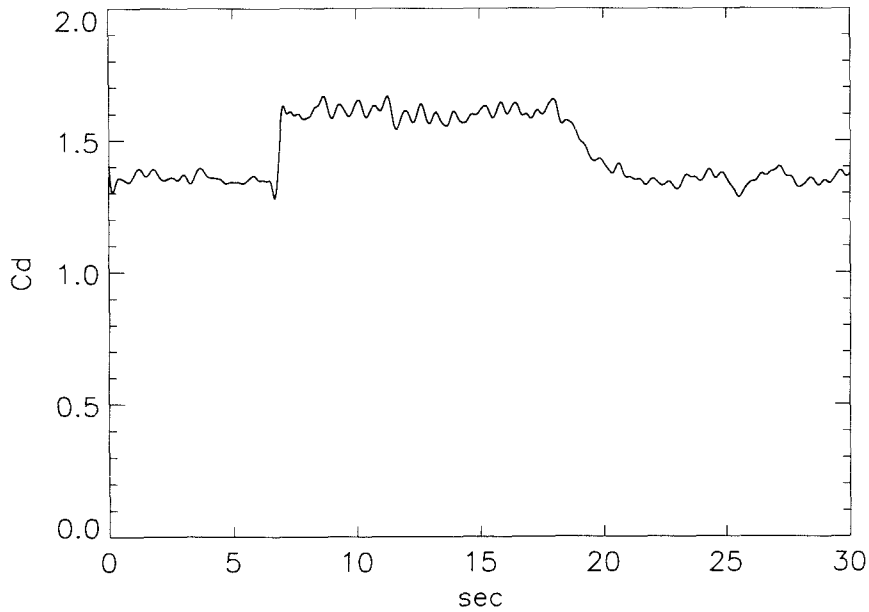

Figure 5-18 Drag trace showing sudden, progressive and random transitions.

6. DPIV Results

6.1 Velocity fields

DPIV was performed for all the cases shown above. Selected velocity vector plots are shown below. These give a quantitative picture of the phenomena discussed in section 5.1.

Three cases are shown, these being for the jet attached to the surface (Mode-1), the jet attached to the plate (Mode-2) and the jet penetrating the wake (Mode-2). In these plots the flow is from left to right past a 4" diameter (10.16 cm) disk. A high speed jet of fluid can clearly be seen adjacent to the surface. Shedding induced by flow of this high speed jet past the cylindrical sting (Figure 6-3) is hypothesized to be the cause of flow induced vibrations for this case.

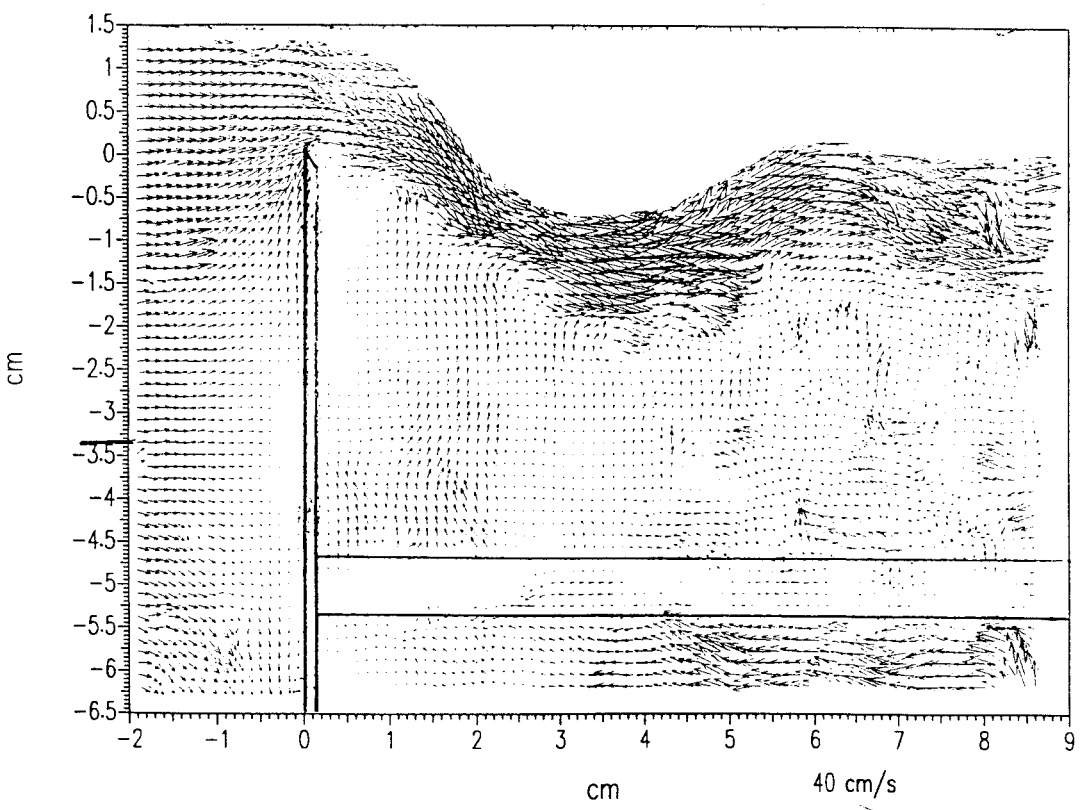

Figure 6-1 Velocity field for a jet attached to the free surface (Mode-1).

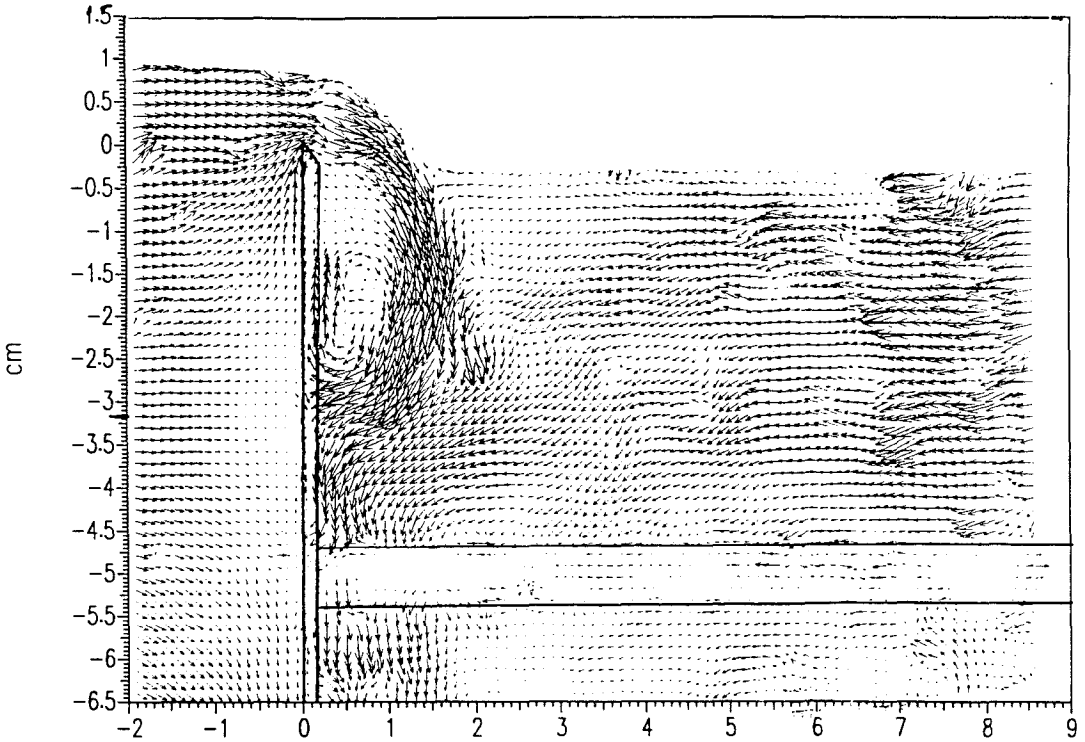

Figure 6-2 Velocity field for a jet attached to the disk (Mode-2).

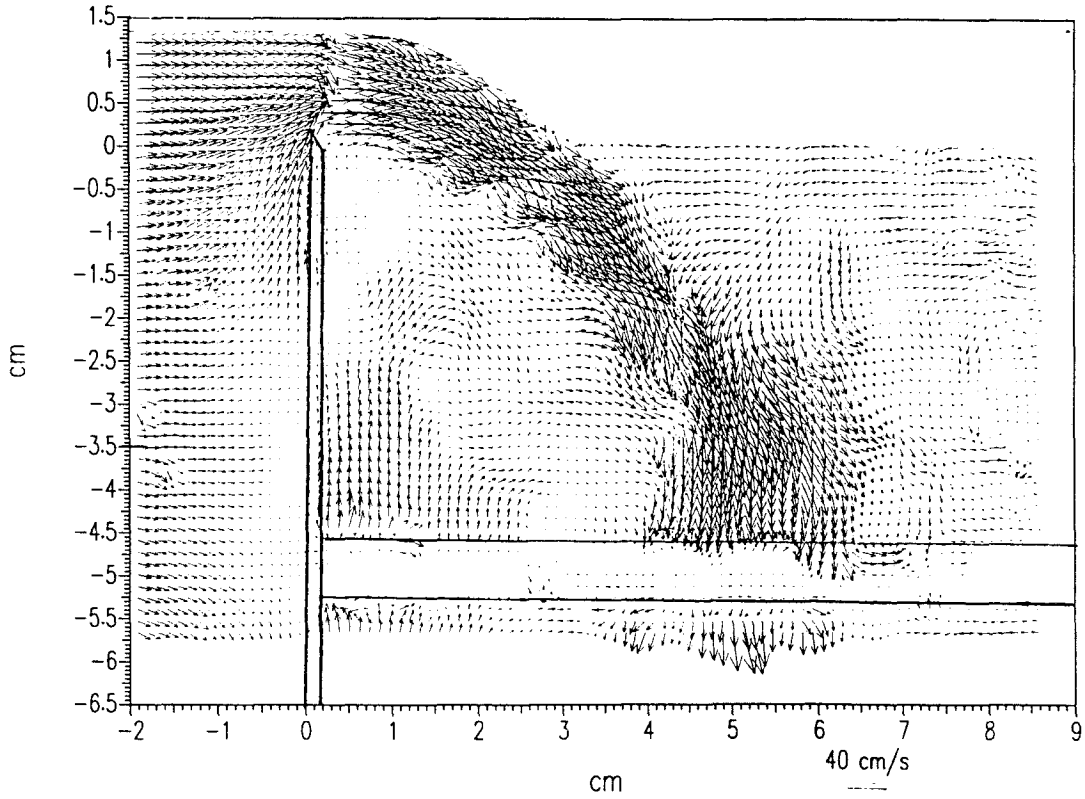

Figure 6-3 Velocity field for a jet penetrating the wake (Mode-2).

6.2 Stagnation point migration

The forward stagnation point for a disk in fully submerged flow is at the geometric center of the disk. The velocity vector plots shown above reveal an interesting feature. It is apparent that the stagnation point moves away from the center of the disk towards its upper edge for decreasing h/d. In the horizontal plane the stagnation point remains on the centerline as may be expected from symmetry. This would be expected to result in a net pitching moment on the disk. This effect would be accentuated when in conjunction with a Mode-2 jet that forms a low pressure region near the top edge, and a stagnation point below the centerline on the rear surface of the disk (Figure 5-11). The location of the front stagnation point is plotted in Figure 6-4, which shows the distance of the stagnation point from the center of the disk as a function of h/d.

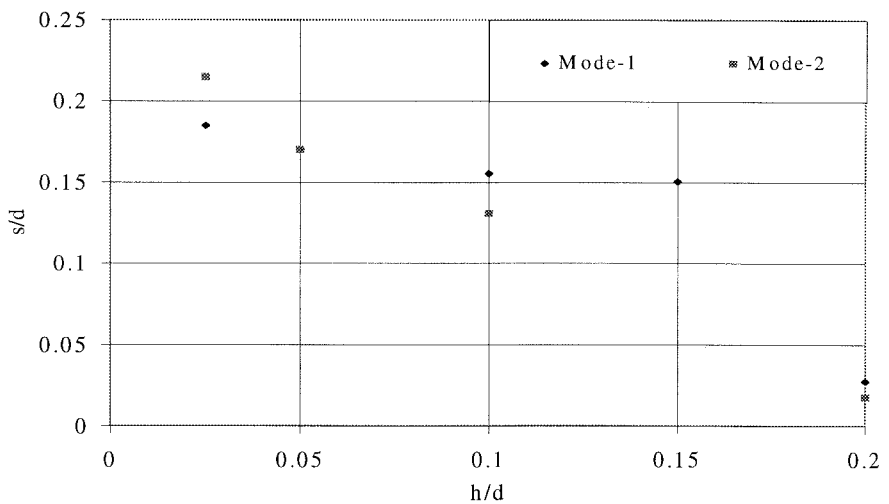

Figure 6-4 Stagnation point migration. 's' is the distance of the stagnation point from the center of the disk.

7. Conclusion

Several new phenomena have been described here. The first is that the free surface causes an increase in drag for an approaching bluff body. In the present set of experiments this increase was as high as 25%. The drag rise comes from two sources, one from surface wave making and one from changes in the pressure in the wake caused by reattachment of the separation streamline. It may be hypothesized that the small increase in drag that occurs in Mode-2 flow with decreasing h/d (Figure 4-7), is largely due to wave making. This is because the wake topology is unchanged though the surface undergoes considerable deformation. The wave making contribution can be seen in Figure 4-7, as the increase in Cd norm from 1 to 1.04 as h/d decreases from 1.5 to 0.02. The subsequent jump in the drag coefficient to Cd norm = 1.25, is due to reattachment of the separation streamline and the consequent appearance of a low pressure region behind the top edge of the disk. During this transition the amplitude of the free surface disturbance does not change significantly, though the patterns formed on the surface change. This indicates that the contribution of wave making to the drag does not change greatly during the transition. The Froude number, based on the gap between the disk and the nominal free surface, is also plotted in the same figure and it may be seen that Cd norm is a maximum for Fr. ~ 1. Havelock (1917) computed the wave making resistance for a subsurface sphere in potential flow. His results predict that the wave making resistance increases as the sphere approaches the surface. They also predict that the wave making resistance is maximum at Fr = 1 (based on the distance from the center of the sphere to the surface). Other potential flow analyses (Miyata, Shikazono and Kanai, 1990) have shown the same effect for circular cylinders. Havelock's analysis also shows that if the maximum increase in wave making resistance for a particular value of d is plotted against U_∞, the curve has a peak. This is consistent with the observation that

the peak in the drag curve at 50 cm/s is greater than that at 40 cm/s and 60 cm/s for the same diameter disk. This observation needs more data to confirm it, specially since the studies quoted are for potential flow, and ~80% of the drag at the peak is due to reattachment of the separation streamline,.

This work further demonstrates that distinctly different wake topologies arise from different initial conditions. This feature of the wake has not been noticed previously. Two Modes are shown to exist in this flow. Mode-1 flow exists around a disk in an infinite medium and is characterized by one or more bores on the free. The introduction of an asymmetric boundary condition in the from of a free surface ultimately modifies the wake by means of a transition to what is referred to as Mode-2 flow. Mode-2 flow is distinguished by a jet of fluid that separates from the edge of the disk and the free surface and penetrates the wake. The jet may, for small values of h/d, reattach itself to the rear of the disk. Mode-2 flow is also characterized by the appearance of a bound vortex whose upstream edge lies behind the top edge of the disk. This core of this vortex may be made visible by air entrained through the surface (Figure 3-5). The low pressure region associated with this core is thought to be the cause of the increased drag in Mode-2.

It is shown that mode switching occurs between these two topologies. These two modes have different regions of stability and can undergo transition from one to the other. The transitions have been described as sudden, progressive and random. The stability of the two modes depends both on initial conditions and h/d. This fact is demonstrated in Figure 4-7 where the drag change associated with the transitions exhibits hysteresis.

The range of velocities (40 cm/s to 60 cm/s) and diameters (3" to 5") were selected because the phenomena of drag rise was clear and measurable in this range. For lower velocities the drag rise was unclear due to noise induced random transitions. Higher velocities were unattainable because of limitations on the maximum load of the force balance. Larger disk

diameters were ruled out by considerations of blockage effects. Lower diameters were ruled out by the minimum force required to get a good signal to noise ratio for the force balance. This limited the Reynolds number to a range of Re = 40,000 to Re = 60,000, so the Reynolds number dependence of this phenomenon was not clarified. However, since the drag curves for two disk diameters at the same velocity (Figures 4-4 to 4-6) approximately fall on each other, it does not appear that the Reynolds number is significant within the range of parameters studied. This is also expected from what is known generally about the weak dependence on Re. of bluff bodies with fixed separation edges.

The parameter h/d is used in this study. It is a better choice than Fr for the abscissa in the drag plots since Fr is undefined for negative values of h and the quantity $U_\infty / \sqrt{gh}$ presents problems as h -> 0. These objections may be overcome by utilizing gh/U_∞^2 as the nondimensional parameter. The Froude number is shown to pass through the critical value of Fr. = 1 around the region of maximum drag rise. It does not serve as an indicator of where transition occurs. Figure 4-5 indicates that transition occurs for h/d = 0.2 corresponding to Fr. ~ 1.1, whereas Figure 4-4 has transition occurring at h/d ~ 1 or Fr. ~ 0.6. The Froude number is based on a global definition of h, i.e. with respect to the nominal surface rather than the local value. This is consistent with the practice elsewhere in fluid mechanics as in the case of transonic flow where the Mach number is based on upstream conditions. However, the transition and hysteresis behavior are governed by local effects at the top of the disk.

Finally comparison is also made with an approaching solid boundary, which shows that the drag still increases, but to a much smaller extent. For this case, surface deformation and reattachment of the separation streamline as seen in Mode-2 flow were not observed. It may be hypothesized that the increase in drag was due to distortion of the basic Mode-1 flow caused by the presence of the solid wall.

REFERENCES

Balligand, H.; Higuchi, H. 1993 Wake of a decelerating disk. *AIAA* Paper 93-1218.

Berger, E.; Scholz, D. 1990 Coherent vortex structures in the wake of a sphere and a circular disk at rest and under forced vibrations. *J. Fluids and Structures* **4**, 231-257.

Blevins, R.D., *Applied Fluid Mechanics Handbook*

Bridges, D.H. 1993 Tip effects on the vortex wake of an axisymmetric body at an angle of attack. *Thesis*, California Institute of Technology

Havelock, T H. 1917 Some cases of wave motion due to a submerged obstacle. *Proc. Roy. Soc.* A. **93**, 119-131.

Hornung, H.G.; Willert, C.E.; Turner, S. 1995 The flow-field downstream of a hydraulic jump. *J. Fluid Mech.* **287**, 299-316.

King, A.C.; Needham, D.J. 1994 The initial development of a jet caused by fluid, body and free surface interaction. *J. Fluid Mech.* **268**, 89-101.

Lisoski, D. 1993 Nominally 2-D flow about a flat plate. *Thesis*, California Institute of Technology

Longuet-Higgins, M.S.1992 Capillary rollers and bores. *J. Fluid Mech.* **240**, 659-679.

Miyata, H., Shikazono, N. & Kanai, M. 1990 Forces on a circular cylinder advancing steadily beneath the free-surface. *Ocean Engng*, **17**, No. 1/2, 81-104.

Miyata, H. & Inui, T. 1984 Nonlinear Ship Waves. *Advances in Applied Mechanics.* **24**

Morton, B.R. 1984 The generation and decay of vorticity. *Geophys. Astrophys. Fluid Dynamics*, **28**, 277-308.

Oguz, H.N.; Prosperetti, A.; 1992 Examples of air-entraining flows. *Phys. Fluids* A **4** (4)

Roshko, A., Steinolfson, A. & Chattoorgoon, V. 1975 Flow forces on a cylinder near a wall or near another cylinder. *Proc. 2nd National Wind Conf. on Wind Eng. Research*

Roshko, A. 1993 Free shear layers, base pressure and bluff body drag. *Proc. Symp. on developments in Fluid Dynamics*, Bangalore, India, Dec. 9-10.

Scullen, D. & Tuck, E.O. 1995 Nonlinear free surface flow computations for submerged cylinders. J. Ship Reseach **39**, No, 3, 185-193.

Sheridan, J., Lin, J.C. & Rockwell, D. 1995 Metastable states of a cylinder wake adjacent to a free surface. *Phys. Fluids* **7** (9) , 2099-2101.

Willert, C.E.; Gharib, M. 1991 Digital particle image velocimetry. *Experiments in Fluids* **10**, 181-193.